



Lung nodule growth measurement and prediction using Multi scale - 3 D- UNet segmentation and shape variance analysis

Sathyamoorthy k.*¹, Ravikumar S.²

¹ Research Scholar, Vel Tech Rangarajan Dr Sagunthala R&D Institute of Science and Technology, India.

² Associate Professor, Vel Tech Rangarajan Dr Sagunthala R&D Institute of Science and Technology, India.

Emails: phdsathyamoorthy@gmail.com; ravikumars@veltech.edu.in;

Abstract

In this work, a statistical model is constructed to forecast the possibility of lung nodules that may grow in the future. This study segments all potential lung nodule candidates using the Multi-scale 3D UNet (M-3D-UNet) method. 34 patients' CT scan series yielded an average of approximately 600 nodule candidates larger than 3 mm, which were then segmented. After removing the arteries, non-nodules and 3D shape variation analysis, 34 actual nodules remained. On actual nodules, the nodule growth Rate (NGR) was calculated in terms of 3D-volume change. Three of the 34 actual nodules had RNG values greater than one, indicating that they were malignant. Compactness, Tissue deficit, Tissue excess, Isotropic Factor and Edge gradient were used to develop the nodule growth predictive measure.

Keywords: cancer prediction; computed tomography; 3D image segmentation; lung nodule; shape measurement.

1. Introduction

Lung cancer ranks third among all cancer types and is the primary cause of cancer-related fatalities, accounting for 1.8 million deaths (18.0%) globally in 2020. Although lung cancer can be lethal, the prognosis is getting better because to efficient diagnosis and therapy. After lung cancer (11.4%), colorectal (10.0%), prostate (7.3%), stomach (5.6%), and lung (11.4%), female breast cancer is now the most often diagnosed malignancy, with an expected 2.3 million new cases (11.7%). Following lung cancer, which accounted for 1.8 million fatalities (18%), the most common cancer-related causes of death were colorectal, liver, stomach, and female breast [1]. It is still difficult for medical personnel to detect cancer. It is yet unknown what causes cancer in the first place or how to treat it completely. If detected early enough, cancer is treatable [2].

Identification of lung nodules on chest CT images is vital given the current status of medical research and practice. The reason for this is the rising prevalence of lung nodules. This directly means that in order to achieve the goal of early lung cancer identification, CAD technologies must be used [2]. To identify areas of the lung affected by cancer, image processing techniques such noise reduction, feature extraction, damaged region identification, and maybe cross-referencing with medical history data on lung cancer are employed [3]. Segmenting lung nodules is crucial for assessing computed tomography (CT) image properties of lung nodules and differentiating between benign and malignant nodules in computer-aided diagnosis methods for lung cancer [4]. To identify potential lung nodules and areas of interest, the segmented lungs can be further utilized, perhaps improving the CT scan classification. However, many modalities have been proposed for effective segmentation of lung nodules which can be used further for better classification [16].

2. Related Work

It is well known that to get an optimal solution for any linear programming problem using the direct simplex algorithm should be processed to be in standard form, the simplex method for solving an LP problem requires the problem to be expressed in the standard form. But not all LP problems appear in the standard form. In many cases, some of the constraints are expressed as inequalities rather than equations;

The lung is porous, lung cancer is exceedingly difficult to detect and diagnose when compared to other tumors. Since lung biopsies are extremely uncomfortable for patients, doctors won't do them unless there is compelling evidence of lung cancer. Generally, patients are advised to have repeat CT scan after a period of 6, 9, or 12 months if the radiologist discovered any abnormalities in the lung CT scan. A biopsy is carried out following the analysis of CT scans at various intervals and according to the degree of illness development (Chheang and Brown, 2013; Gould et al., 2013).

Qianqian Zhang et. al. (2019) [5] proposed the deep CNN model's architecture, including specifics like network dimension, convolutional layer designs, and training methodologies, is most likely included in the publication. It could also include information on the preprocessing techniques used on the CT images and the dataset utilized for training and validation. The deep CNN model's performance is probably compared to other approaches or human experts in terms of sensitivity, specificity, accuracy, and other pertinent metrics. The study may also go into the suggested approach's shortcomings and its clinical ramifications.

Armato, S.G. et. al. (2004) [6] proposed a lung segmentation in lung CT images and its effects on computer-aided diagnosis (CAD) appear to be covered in this work. In order to facilitate further analysis, such as CAD, automated lung segmentation—which separates the lungs from the surrounding tissues and structures—is an essential stage in the processing of thoracic CT images. Precise lung segmentation has a major effect on CAD systems. Precise anatomical limits and a decrease in the number of false positives and number of false negatives can improve the efficiency of CAD algorithms. Accurate segmentation enables CAD systems to identify and describe lung abnormalities—such as masses, nodules, and other lesions—better, supporting radiologists in their diagnostic and treatment choices.

Alilou, M. et. al. [7] had proposed the methodical strategy for the automated identification of nodules in the lungs in lung CT scans is probably presented in this study. The architecture put forth in the article may include a number of steps and techniques meant to precisely locate and describe nodules in lung CT images. Preprocessing to improve picture quality, segmentation of the lungs to separate the lung area, candidate nodule detection utilizing methods such as extraction and classification of features, and false positive minimization to reduce false positives are some examples of these phases.

Jo, H.H. et. al. [8] proposed the research presents a technique for precisely recording lung nodules over several CT images obtained at various intervals. In longitudinal research or patient monitoring, this registration procedure is essential for tracking the development or regression of lesions over time.

Krishnamurthy, S et. al. [9] are seems to be concentrated on improving the techniques for detecting lung cancer by using a thorough strategy that includes shape variance analysis and three-dimensional lung nodule segmentation. The technical aspects of the identification and analysis procedures, which might include statistical analysis, processing of images techniques, and machine learning algorithms, are probably covered in the article. It could also provide data—possibly from trials done on clinical datasets—that show how well the suggested strategy works in terms of precision, specificity, sensitivity, and false positive reduction.

Ko, J.P., Berman et. al. [10] These method for growth rate evaluation, volumetric analysis, and nodule segmentation, as well as the difficulties and factors to be taken into account, are probably covered in the article. It could also provide information on the rates of growth of nodules in the lungs in the patient group under investigation, together with information on potential growth-influencing variables and consequences for patient care and prognosis. All things considered, the study advances our knowledge of lung nodule behavior and offers insightful information about patient nodule growth patterns. This information can help with clinical decision-making, risk assessment, and treatment planning for patients with suspected or confirmed lung lesions.

Yifan Wang et. al. [11] In this work, a hybrid deep learning model for lung nodule segmentation with different shapes, sizes, margins, and opacities will be developed. a dataset of 847 instances of lung nodules that was obtained through the LIDC and painstakingly labeled by a minimum of two radiologists. Two novel U-DL model were built using the fundamental symmetric U-shaped U-Net design and then enlarged to a total of six of convolutional layers. The two U-DL methods were then combined using a combined layer to produce the H-DL models. Our H-DL model has an average three-dimensional Dice factor & average JI of 0.750 and 0.131, respectively.

Joana Rocha et.al [12] In this method in order to segment pulmonary nodules in computed tomography images, three different approaches are proposed in this research. The methods are Deep Learning-based and use the U-Net and SegU-Net, a brand-new network, to accomplish the same task. In order to determine the most effective technique for improving nodule characterisation, their performances are compared in this paper. 2653 nodules taken from the LIDC database were utilized by all techniques, yielding Dice scores for the SBF, U-Net, and SegUNet of 0.663, 0.830, and 0.823, respectively.

Hasegawa, M. et. al. [13] The goal of the project is to better understand the early development dynamics of tiny pulmonary nodules by using sophisticated three-dimensional computer-aided analytic techniques. Most likely, a retrospective examination of CT scans from individuals with tiny pulmonary nodules was carried out by the researchers. They could have measured the nodules' volume, morphological characteristics, and size over time using three-dimensional computer-aided analytic methods.

2.1 Dataset

The CT data of identical slice thickness for 34 individuals is available in the open-source repository VALCANO (Volcano, 2009), from which the pictures used in this work were retrieved. With GE Medical and Philips CT scanners with varying X-ray tube current and exposure, a series of CT scans were performed for each patient at various intervals. The position of the nodules is known, however the time interval between the two scans is not stated. This investigation involved the analysis of 1712 cross-sections of CT scans from 34 instances. Each image is 512 x 512 inches in size, with a pixel spacing of 0.76 mm in both directions (x and y), and a 16-bit gray resolution. The exposure duration is 553 ms, and the current dose for the X-ray tube is 80 mA. In order to protect patient privacy, the name of the individual's DICOM tag (0010,0010) has been changed to SC00xx. Additionally, the individual's age and gender DICOM tags (0010,0030) and (0010,0040) have been deleted from the database.

3. Lung Nodule Segmentation

A nodule refers to a tissue mass found within the lung parenchyma region. Nodules can exhibit various characteristics and classifications based on their location and appearance. Well-circumscribed nodules are typically round and situated deep within the lung parenchyma. They maintain distinct boundaries from surrounding tissues [14]. Vascularized nodules are associated with blood vessels within the lung area, indicating a vascular connection. Pleural-tail nodules present as tail-like formations attached to the lung walls, while juxta-pleural nodules have significant connections to the lung wall region [15]. These classifications provide insight into the characteristics and potential behaviour of nodules within the lung parenchyma, aiding in diagnosis and treatment decisions.

3.1 Segmentation of Lung Nodules in CT Images Using M-3D-UNet

Here M-3D-UNet is used to segment the input CT images that are provided as detailed in Figure 1. The input for the specified M-3D-UNet model is the raw CT images that are gathered from the volcano dataset. Multi-scaling is achieved by partitioning the 3D-UNet's convolutional layer into many dimensions and feeding the input to each of the convolutional layers with a distinct dimension. The convolutional layer of the M-3D UNet is split into convolutional layers of different dimensions in order to create the M-3D-UNet. Subsequently, every unique dimensions convolutional layer processes the input. Within the M-3D-UNet, processes including feature concatenation, down sampling, MHA, and up sampling occur [17]. Ultimately, the M-3D-UNet's segmentation head provides the segmented image as shown in Figure 1.

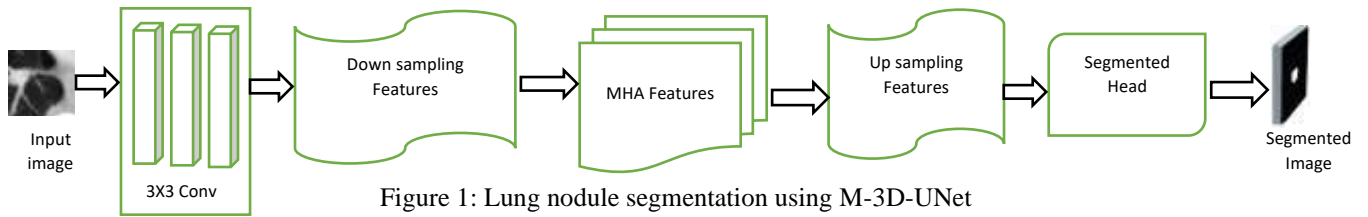


Figure 1: Lung nodule segmentation using M-3D-UNet

The method for segmenting lung nodules using a Multi-scale 3D UNet model is described in Algorithm 1. The first step is the preparation of the input data, which involves gathering the raw CT images from the volcanic dataset. In order to configure the M-3D-UNet model, the 3D-Unet's convolutional layer is divided into numerous dimensions, where N is the number of dimensions[20]. Following that, the input CT scans are divided into various dimensions and supplied to the appropriate convolutional layers inside the M-3D-UNet model. Processing in the M-3D-UNet includes concatenating features, using Multi-Head Attention (MHA) to capture contextual information and long-range dependencies in various lung imaging areas. This can be useful for dividing out areas or complicated structures that have different properties, such as lung tissue, blood arteries, or nodules. Followed by down sampling to decrease spatial resolution, and upsampling to enhance spatial resolution. Lastly, segmentation is carried out using the M-3D-UNet model's segmentation head to produce the segmented picture as the output [19][26][27].

Algorithm 1: SEGMENTATION OF LUNG NODULE USING MULTI-SCALE 3D UNET

1. Input Data Preparation:

- Gather raw CT images from the volcano dataset.

2. Model Architecture Setup:

- Configure the M-3D-UNet model architecture.

Divide the 3D-Unet's convolutional layer into multiple dimensions:

- Let N be the number of dimensions.

Create distinct convolutional layers for each dimension to form the M-3D-UNet model:

- ConvLayer _{i} represents the i -th convolutional layer for $i = 1$ to N .

3. Multi-Scaling Input:

Partition the input CT images into different dimensions:

- Input_CT _{i} represents the input CT image for the i -th dimension.

Feed each dimension of the input to the corresponding convolutional layer in the M-3D-UNet model:

- ConvLayer _{i} (Input_CT _{i}) represents the output of ConvLayer _{i} for the i -th dimension.

4. Processing within M-3D-UNet:

Feature concatenation:

- Concatenate features extracted from different dimensions:

- Concatenated_Features = Concatenate(ConvLayer₁(Input_CT₁), ..., ConvLayer _{N} (Input_CT _{N})).

Downsampling:

- Reduce the spatial resolution of feature maps:

- Downsampling_Features = Downsampling(ConvLayer₁(Input_CT₁), ..., ConvLayer _{N} (Input_CT _{N})).

Multi-Head Attention (MHA):

- Apply attention mechanism to capture long-range dependencies:

- MHA_Features = MHA(Downsampling_Features).

Upsampling:

- Increase the spatial resolution of feature maps:

- Upsampled_Features = Upsampling(MHA_Features).

5. Segmentation:

Utilize the segmentation head of the M-3D-UNet model to obtain the segmented image:

- Segmented_Image = Segmentation_Head(Upsampled_Features).

6. Output:

- Obtain the segmented image as the output of the M-3D-UNet model.

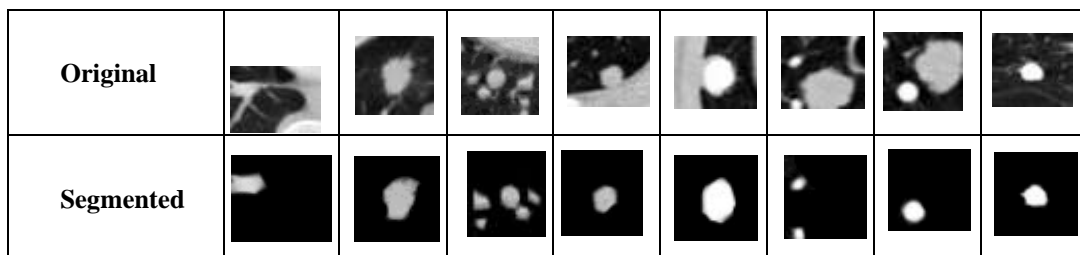


Figure 2. Segmentation Output

Upper row in Figure 2 shows the original, unprocessed lung images obtained from medical imaging modalities of CT scans. Raw lung images depict the anatomical structures of the lungs without any specific delineation or highlighting of regions of interest and the segmented lung images generated after applying image segmentation techniques to the raw lung images. And the above figure depicts a visual comparison between the original raw lung images and the processed final segmented images, the segmentation technique in isolating the regions of interest within the lungs.

4. Morphology analysis of nodules

In morphological methods that detect related components in a picture after segmentation are often employed. For this reason, the linked component labeling method is one of the most used morphological algorithms. After the arteries are removed, as was covered in Section 1, the remaining suspected nodule candidates were found. The radiologist typically uses the lung nodule's developing nature to determine whether it is malignant. It is necessary to measure the lung nodule's growth in terms of volume rather than area. A tiny alteration in the nodule's 2D area could have a significant impact on its 3D volume (). The connected component algorithm iterates across each pixel within the binary image, assessing whether its neighbouring pixels also belong to the identical connected component. If a pixel is found to be part of a newly linked component, it is given a label. It is given the label of the linked component if it is a part of an already-existing component. The algorithm tracks the labels that are applied to every linked component. The method groups pixels with the same label to identify different related components once every pixel in the picture has been classified. Therefore, the volume of each final nodule candidate is calculated in our work using equation (1).

$$VOL = \sum(\text{from } x = 1 \text{ to } m) \sum(\text{from } y = 1 \text{ to } n) \sum(\text{from } z = 1 \text{ to } k) \text{node}(x,y,z) \dots\dots\dots (1)$$

where k represents the number of images containing a single nodule.

The volumes of final nodules are calculated using both scans of each patient taken at various time interims. Equation (2) characterizes the quantitative measure of volume change as the rate of nodule growth.

$$NGR = \frac{VOL_2 - VOL_1}{VOL_1} \dots\dots\dots (2)$$

Where VOL1 is the volume of the nodule in an previous scan and VOL2 is the volume of the nodules in a latter scan.

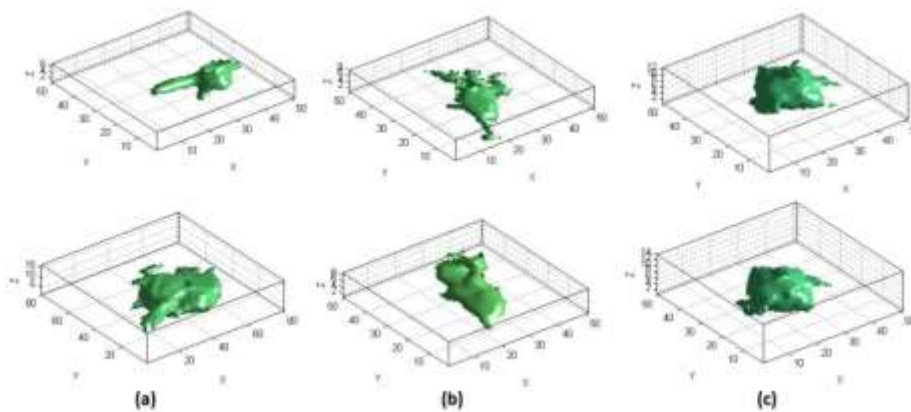


Figure 3: 3-D visualisation of patient case final nodule candidate, which segmented from the CT scans. In figure (3), the nodules segmented from the earlier and later scans are shown patient case. Figure 3(a) and 3(b) show the nodules segmented from the earlier scan (first row images). These nodules' surfaces are not smooth. Few tissue parts are coming out of the nodule surface in a radial direction, but in Figure 3(c), the tissue parts coming out of the nodule surface are minimal and the surface seems smooth. The latter scans of all of these cases revealed that the first two cases illustrated in Figures 3(a) and 3(b) grew in the future, however the nodule in Figure 3(c) did not expand [14]. The characteristics of nodules segmented from previous images are utilized as a quantitative method to predict nodule growth [9].

5. Predicting nodule growth

The nodules are cancerous and have the potential to expand. In routine practice, doctors compare two scans obtained at reasonable intervals to determine whether to recommend a nodule growth (Yankelevitz and

Henschke, 1997). In this portion of the work, we are proposing a method to identify nodules from the previous CT scan that may potential to grow.

Based on the observations of Figure (3), the amount of these nodules has significantly increased between earlier and later images of scan. This notable increase suggests potentially aggressive nature of growth and may give rise to worries regarding the nodules' quick progression or malignancy (3a). The growth rate indicates gradual changes in the nodule over time, even if it is not noticeable compared to those in the "large growth" group (3b). The nodules' stability indicates that there was no discernible development or advancement (No development) over the studied time (3c).

In order to predict the nodules which are likely to expand in the future, the quantitative measures like compactness (C), Tissue deficit (TD), Tissue excess (TS), Isotropic Factor (IF) and Edge Gradient (EG) are computed to characterize and analyze features or structures within images, providing valuable insights into their properties, distributions, and relationships.

Compactness (C)

The degree to which an object is dense or tightly packed in relation to its volume or surface area is measured by its compactness. The shape's degree of branchiness is determined by its compactness is shown in Figure 4. Compactness for a given 2D shape can be found using the following formula, where A represents the enclosed area and P the perimeter in Equation (3).

$$C = (4 * \pi * A) / P^2 \dots\dots\dots (3)$$



Figure 4: Compactness (C)

Tissue Deficit (TD)

A tissue deficit could potentially refer to a measure or calculation related to the deficit or loss of tissue within a nodule. This could involve quantifying the extent to which tissue density is reduced or absent within the nodule compared to surrounding healthy tissue.

This is the area that separates the form and the largest enclosing circle that is centered around the form's center of gravity is shown in Figure 5. Where C_c is the circumscribed circle area for the shape of area A, then TD can be found using equation (4).

$$TD = \frac{C_c - A}{C_c} \dots\dots\dots (4)$$



Figure 5: Tissue Deficit (TD)

Tissue Excess (TE)

The Tissue excess (TE) represents the area difference between the form and the minimum enclosing circle that is centered around the form's center of gravity as shown in Figure 6. If we take C_i to be the area of the inscribed circle for a shape of area A, then TE can be found using equation (5),

$$TE = \frac{A-C_i}{C_i} \dots\dots\dots (5)$$

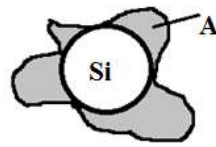


Figure 6: Tissue Excess (TE)

Isotropic Factor (IF)

The process of obtaining images with equal quality in all three spatial dimensions. This is usually accomplished by employing voxels of similar sizes in each dimension. This characteristic reflects how regular the form is around its center of gravity and how isotropic the pattern is shown in figure 7. If we assume that the lowest radius of a given 2D shape is R_m and the maximum radius is R_M , then the IF parameter is given by equation (6)

$$IF = \frac{R_m}{R_M} \dots\dots\dots (6)$$

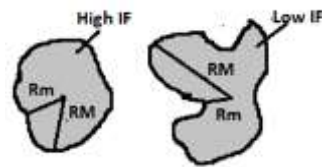


Figure 7: Isotropic Factor (IF)

Edge Gradient (EG)

In order to estimate the total edge gradient, the algorithms first calculate the rate of change of pixel intensity or colour in both the horizontal and vertical directions as shown in Figure 8. These values are then combined by summing the individual gradient magnitudes along the edge and dividing by the length of the gradient vector, it provides a measure of the average steepness or strength of the edge gradient as given by equation (7).

$$EG = \sum_{k=1}^p \left[\frac{\text{Mag}(\text{gradient}(f(i,j)))}{\text{Length}(X_{\text{gradient}})} \right]_k \dots\dots\dots (7)$$

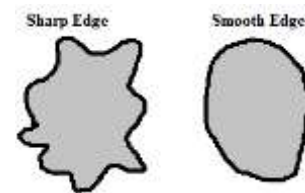


Figure 8: Edge Gradient (EG)

6. Results

Every lung-imaging slice can be segmented using the M-3D-UNet algorithm with effectiveness, and Figure 2 displays the candidates for suspected nodules from a single CT slice image. The nodule candidates with a size greater than 3 mm were considered for further analysis. The nodule growth rate is computed using Equation (2) and the values are tabulated in Table 1. Table 2 lists the growth prediction metrics for the nodule that were calculated from a previous CT scan.

Table 1: Nodule growth rate in two scans of same patient

Case No.	Database Case ID	Volume Scan 1(Cubic mm)	Volume Scan 2 (Cubic mm)	Volume Diff	NGR
----------	------------------	-------------------------	--------------------------	-------------	-----

1	1	553.61	8646.90	8093.29	14.619
2	2	1852.41	2263.66	411.26	0.222
3	6	83.48	205.63	122.15	1.463
4	7	130.93	159.05	28.12	0.215
5	8	79.09	79.97	0.88	0.011
6	0 1	1309.34	1325.16	15.82	0.012
7	1 1	4956.15	5246.14	289.99	0.059
8	3 1	7203.11	7685.55	482.43	0.067
9	5 1	392.80	567.67	174.87	0.445
10	6 1	249.57	279.44	29.88	0.120
11	8 1	3259.28	3373.52	114.24	0.035
12	0 2	1177.53	1188.95	11.42	0.010
13	1 2	1967.52	1962.25	-5.27	0.003
14	3 2	2466.65	2663.49	196.84	0.080
15	4 2	817.24	791.75	-25.48	0.032
16	5 2	1304.94	1723.23	418.29	0.321
17	8 2	840.09	1177.53	337.44	0.402
18	9 2	56.24	58.00	1.76	0.031
19	2 3	98.42	108.97	10.55	0.107
20	3 3	565.04	570.31	5.27	0.009
21	4 3	93.15	140.60	47.45	0.509
22	6 3	903.36	964.87	61.51	0.068
23	7 3	1597.57	2135.36	537.80	0.337
24	8 3	1530.78	1612.51	81.72	0.053
25	9 3	1687.20	2225.87	538.67	0.319
26	0 4	679.27	838.33	159.05	0.234
27	1 4	1086.14	1376.12	289.99	0.267
28	2 4	536.92	746.94	210.02	0.391
29	4 4	606.34	1191.59	585.25	0.965
30	5 4	761.00	1074.71	313.71	0.412
31	4	119.51	130.93	11.42	0.096

	6					
32	7	4	1483.33	1855.04	371.71	0.251
33	8	4	573.82	334.80	-239.02	0.714
34	9	4	3761.05	4349.81	588.76	0.157

In figure 9, Lung nodule growth rates are classified as high, medium, or low growth status according to how quickly they increase over time. Nodules with a high growth rate usually increase quickly, sometimes doubling in size in a short amount of time. This might raise worries about malignancy and call for vigilant observation or prompt action. Nodules with a medium growth rate exhibit a gradual yet noticeable rise in size, whilst those with a low growth rate show little to no expansion. Even though nodules with low growth rates are less likely to be malignant, all categories need to be monitored for stability or changes that could be signs of cancer. Accurate diagnosis and treatment depend on a number of factors, including nodule size, morphology, patient history, and additional imaging characteristics.

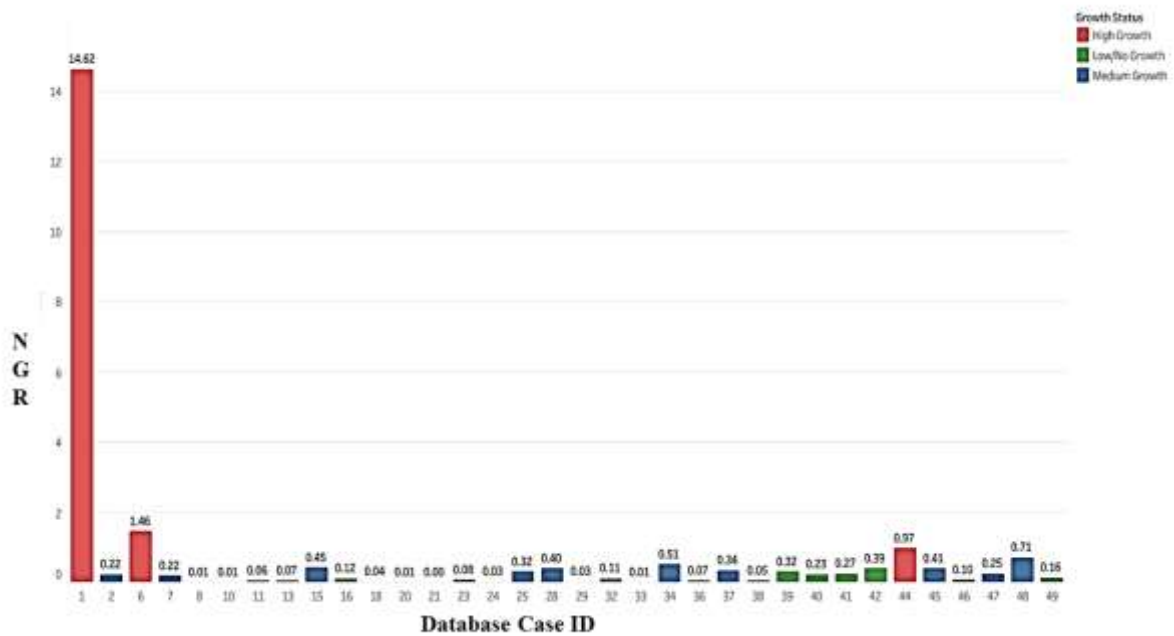


Figure 9: Classification of NGR with high, Medium, Low Growth status

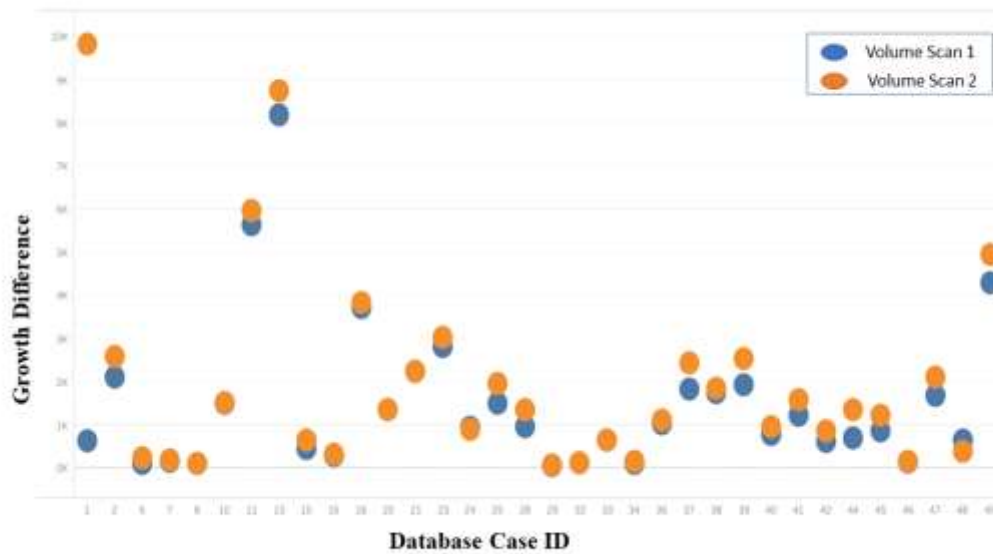


Figure 10: Growth difference between scan 1 and Scan 2

Figure (10) shows the growth variance between two lung nodule scans is to compare the nodule sizes on each scan and compute the rate of change throughout the interim interval.

Table 2: Lung nodule predictive measures

Case No.	Database Case ID	Compactness (C)	Tissue Deficit (TD)	Tissue Excess (TE)	Isotropic Factor (IF)	Edge Gradient (EG)
1	1	0.15	0.69	0.8	0.2	0.22
2	2	0.66	0.3	0.35	0.69	0.10
3	6	0.22	0.56	0.73	0.19	0.22
4	7	0.67	0.27	0.33	0.71	0.07
5	8	0.89	0.16	0.12	0.89	0.02
6	10	0.91	0.15	0.11	0.91	0.08
7	11	0.87	0.19	0.21	0.87	0.18
8	13	0.85	0.19	0.21	0.87	0.22
9	15	0.49	0.46	0.52	0.28	0.17
10	16	0.79	0.23	0.26	0.81	0.07
11	18	0.9	0.16	0.14	0.9	0.09
12	20	0.95	0.13	0.09	0.95	0.08
13	21	0.97	0.1	0.06	0.99	0.20
14	23	0.81	0.21	0.24	0.79	0.18
15	24	0.88	0.18	0.14	0.9	0.20
16	25	0.56	0.37	0.46	0.5	0.19
17	28	0.43	0.45	0.55	0.25	0.19
18	29	0.9	0.16	0.13	0.91	0.03

19	32	0.81	0.21	0.25	0.8	0.06
20	33	0.98	0.09	0.05	0.99	0.04
21	34	0.33	0.47	0.57	0.23	0.19
22	36	0.84	0.19	0.22	0.85	0.08
23	37	0.54	0.42	0.48	0.45	0.19
24	38	0.86	0.18	0.2	0.88	0.08
25	39	0.6	0.35	0.43	0.54	0.22
26	40	0.65	0.3	0.37	0.69	0.16
27	41	0.64	0.33	0.39	0.67	0.18
28	42	0.55	0.43	0.47	0.45	0.19
29	44	0.22	0.57	0.79	0.16	0.20
30	45	0.46	0.52	0.55	0.27	0.19
31	46	0.8	0.2	0.25	0.8	0.07
32	47	0.66	0.3	0.36	0.7	0.21
33	48	0.29	0.53	0.64	0.21	0.19
34	49	0.75	0.25	0.3	0.78	0.22

Parameters such as compactness, tissue deficit, tissue excess, isotropic factor, and edge gradient play pivotal roles in predicting nodule growth in lung imaging analysis. Compactness refers to the density of the nodule, with more compact nodules often indicating a higher likelihood of malignancy. Tissue deficit and excess refer to deviations from normal lung tissue density, with deficits suggesting potential malignancy and excess potentially indicating inflammation or benign processes. The isotropic factor relates to the uniformity of density within the nodule, with less uniformity often associated with malignancy. Edge gradient assesses the sharpness of the nodule's border, with irregular or speculated edges raising concerns for malignancy. Integrating these parameters enables a comprehensive evaluation of nodule characteristics, aiding in the prediction of growth behavior and guiding clinical decisions regarding further investigation or intervention as shown in Figure 11.

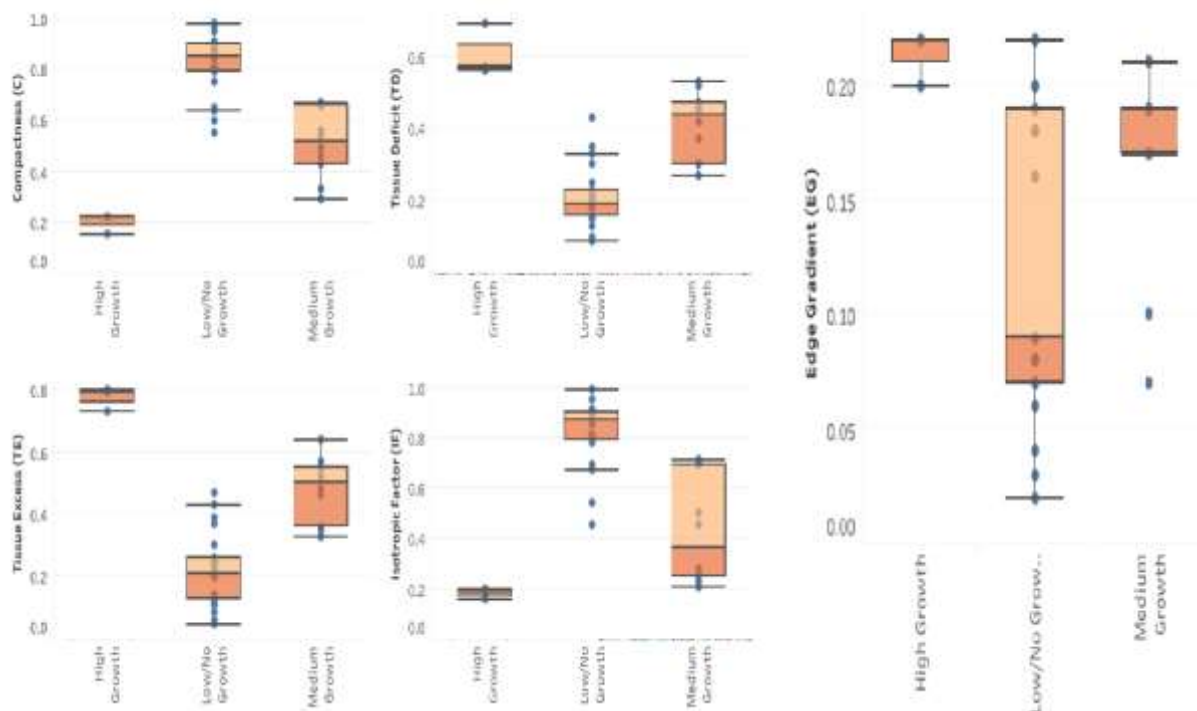


Figure 11: Parameters for predicting nodule growth

7. Discussion

The features of nodules with the potential to expand in the future are predicted by comparing the 17 nodules with very little or no growth to the three nodules with significant growth and the 14 nodules with medium growth from the previous CT scan. The isotropic factor, compactness, mass surplus, and mass deficiency are used to gauge the nodule growth projection. Table 2 tabulates these values, which are calculated for each of the 34 nodules. A greater increase was seen in the three nodules with $C < 0.2$, $IF < 0.2$, $TD > 0.5$, $TE > 0.7$, and $EG < 0.25$. The C ranged from 0.2 to 0.70, the IF from 0.2 to 0.69, the TD from 0.22 to 0.52, the TE from 0.30 to 0.72, and the EG from 0.10 to 0.19 of the 14 nodules with medium growth. Ultimately, the $CO > 0.75$, $IF > 0.79$, $TD < 0.21$, $TE < 0.25$, and $EG < 0.10$ are the values for the 17 nodules that showed very little to no growth. Consequently, there may be room for growth in nodules with low compactness, low isotropic factor, high mass deficit, and high mass surplus values. The analysis and testing of the study is limited to the 34 patient cases in the VOLCANO database. By validating, the methods suggested by this study across several different databases, this issue could be addressed in subsequent work, hence increasing the work's dependability. Figure 12 and 13 depicts the average parametric measurements of the segmented lung nodules for the category of Medium Growth, Low/No growth and High Growth.

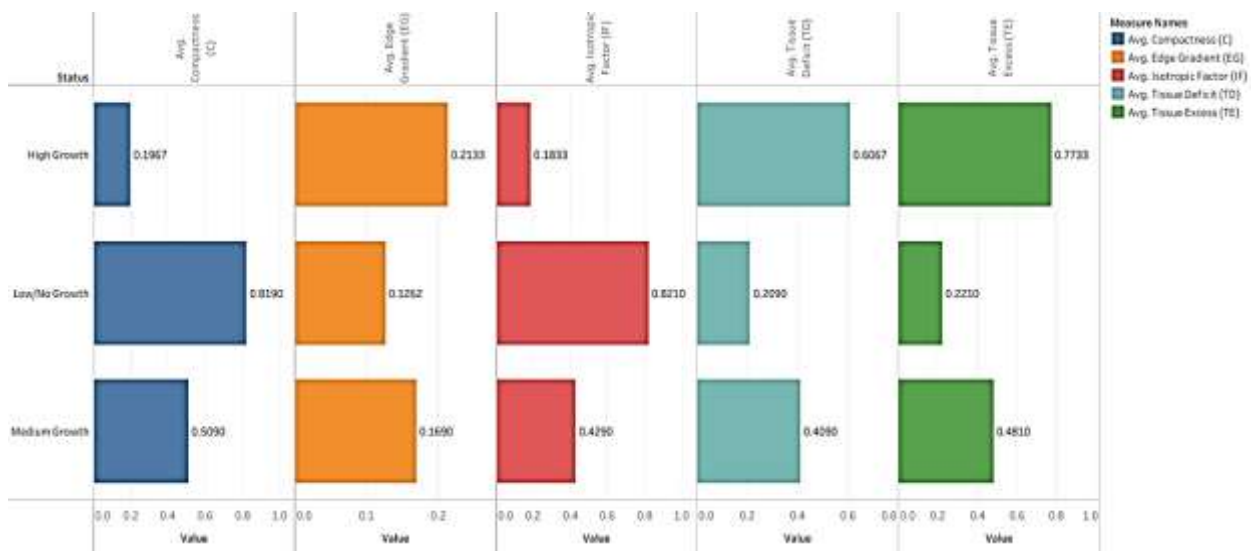


Figure 12: Average parametric measurement for lung nodule

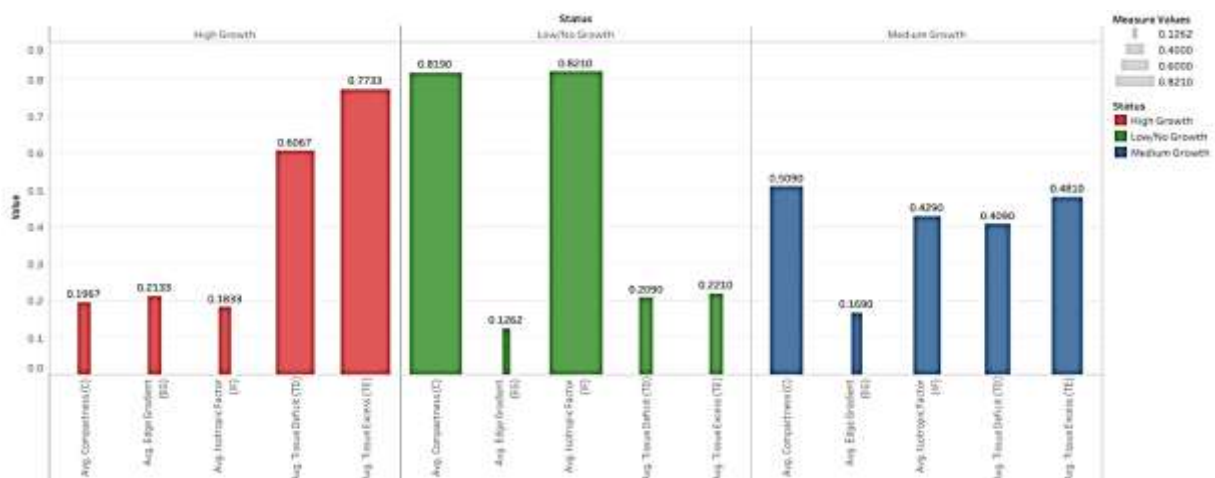


Figure 13: Average growth status parametric measurement w.r.t value

8. Conclusion

This paper developed an efficient system to predict lung nodule development. This work implements the M-3 D UNet method, which segments all potential nodule candidates larger than 3 mm. By quantitatively comparing the amount of a nodule segmented using the CT scan recorded at two different times for the same patient, the nodule growth rate was calculated. Three of the 34 actual nodules that were segmented in this experiment had NGR values greater than 1, indicating that they were malignant nodules. Between 0.2 to 0.8 NGR was found in 14 nodules; more scans may be necessary to determine the malignancy of these nodules. Of the 17 nodules that are left, 7 have nearly zero NGR, while the other 10 have RNGs of around 0.1. These nodules may need to have follow-up scans depending on the patient's lifestyle and surroundings. The prediction measure for nodule growth was calculated using the following terms: edge gradient, compactness, isotropic factor, tissue excess, and deficiency. Based on the correlation between these measurements and RNG, it was determined that nodule with low C, high TD, high TE, low IF, and high EG had the greatest potential for growth.

Funding: "This research received no external funding"

Conflicts of Interest: "The authors declare no conflict of interest."

References

- [1] Sung H, Ferlay J, Siegel RL, Laversanne M, Soerjomataram I, Jemal A, Bray F. Global Cancer Statistics 2020: GLOBOCAN Estimates of Incidence and Mortality Worldwide for 36 Cancers in 185 Countries. *CA Cancer J Clin.* 2021 May;71(3):209-249. doi: 10.3322/caac.21660. Epub 2021 Feb 4. PMID: 33538338.
- [2] Ahmed Medjahed S., AitSaadi T., Benyettou A., Ouali M. Kernel-based learning and feature selection analysis for cancer diagnosis. *Applied Soft Computing* . 2017;51:39–48. doi: 10.1016/j.asoc.2016.12.010.
- [3] Nageswaran S, Arunkumar G, Bisht AK, Mewada S, Kumar JNVRS, Jawarneh M, Asenso E. Lung Cancer Classification and Prediction Using Machine Learning and Image Processing. *Biomed Res Int.* 2022 Aug 22;2022:1755460. doi: 10.1155/2022/1755460. Retraction in: *Biomed Res Int.* 2024 Jan 9;2024:9851527. PMID: 36046454; PMCID: PMC9424001.
- [4] Kido S, Kidera S, Hirano Y, Mabu S, Kamiya T, Tanaka N, Suzuki Y, Yanagawa M, Tomiyama N. Segmentation of Lung Nodules on CT Images Using a Nested Three-Dimensional Fully Connected Convolutional Network. *Front Artif Intell.* 2022 Feb 17;5:782225. doi: 10.3389/frai.2022.782225. PMID: 35252849; PMCID: PMC8892185.
- [5] Qianqian Zhang, Haifeng Wang, Sang Won Yoon, Daehan Won, and Krishnaswami Srihari, "Lung Nodule Diagnosis on 3D Computed Tomography Images Using Deep Convolutional Neural Networks," *Procedia Manufacturing*, Vol. 39, pp. 363-370, 2019.
- [6] Armato, S.G. and Sensakovic, W.F. (2004) 'Automated lung segmentation for thoracic CT: impact on computer-aided diagnosis', *Academic Radiology*, Vol. 11, No. 9, pp.1011–1021.
- [7] Alilou, M., Kovalev, V., Snezhko, E. and Taimouri, V. (2014) 'A comprehensive framework for automatic detection of pulmonary nodules in lung CT images', *Image Analysis & Stereology*, Vol. 33, No. 1, pp.13–27
- [8] Jo, H.H., Hong, H. and Goo, J.M. (2014) 'Pulmonary nodule registration in serial CT scans using global rib matching and nodule template matching', *Computers in Biology and Medicine*, Vol. 45, pp.87–97.
- [9] Krishnamurthy, S., Narasimhan, G. and Rengasamy, U. (2016) 'Three-dimensional lung nodule segmentation and shape variance analysis to detect lung cancer with reduced false positives', *Proceedings of the Institution of Mechanical Engineers, Part H: Journal of Engineering in Medicine*, Vol. 230, No. 1, pp.58–70.
- [10] Ko, J.P., Berman, E.J., Kaur, M., Babb, J.S., Bomsztyk, E., Greenberg, A.K., Naidich, D.P. and Rusinek, H. (2012) 'Pulmonary nodules: growth rate assessment in patients by using serial CT and three-dimensional volumetry', *Radiology*, Vol. 262, No. 2, pp.662–671.
- [11] Yifan Wang; Chuan Zhou; Heang-Ping Chan; Lubomir M Hadjiiski; Amer Chughtai; Ella A Kazerooni; "Hybrid U-Net-based Deep Learning Model for Volume Segmentation of Lung Nodules in CT Images", *MEDICAL PHYSICS*, 2022
- [12] Joana Rocha, Ant ́onio Cunha, Ana Maria Mendonca, Conventional Filtering Versus U-Net Based Models for Pulmonary Nodule Segmentation in CT Images, *Journal of Medical Systems* (2020) 44:81
- [13] Hasegawa, M., Sone, S., Takashima, S., et al. "Early growth of small pulmonary nodules measured by three-dimensional computer-aided analysis." *Journal of Chest*, 2002.

- [14] Sathya Preiya V, Kumar VDA. Deep Learning-Based Classification and Feature Extraction for Predicting Pathogenesis of Foot Ulcers in Patients with Diabetes. *Diagnostics*. 2023; 13(12):1983. <https://doi.org/10.3390/diagnostics13121983>.
- [15] Kumar, T.S. and Ganesh, E.N. (2013) 'Proposed technique for accurate detection/segmentation of lung nodules using spline wavelet techniques', *International Journal of Biomedical Science*, Vol. 9, No. 1, pp.9–17.
- [16] N. Lee, A. F. Laine, G. Mrquez, J. M. Levsky, and J. K. Gohagan, "Potential of Computer-Aided Diagnosis to Improve CT Lung Cancer Screening," *IEEE Reviews in Biomedical Engineering*, vol. 2, pp. 136-146, 2009.
- [17] Min Li, Xiaojian Ma, Chen Chen, Yushuai Yuan, Shuailei Zhang, Ziwei Yan, Cheng Chen, Fangfang Chen, Yujie Bai, Panyun Zhou, Xiaoyi Lv, Mingrui Ma, "Research on the Auxiliary Classification and Diagnosis of Lung Cancer Subtypes Based on Histopathological Images," *IEEE Access*, Vol. 9, 2021.
- [18] Balakrishnan C, Ambeth Kumar VD. IoT-Enabled Classification of Echocardiogram Images for Cardiovascular Disease Risk Prediction with Pre-Trained Recurrent Convolutional Neural Networks. *Diagnostics (Basel)*. 2023 Feb 18;13(4):775. doi: 10.3390/diagnostics13040775. PMID: 36832263; PMCID: PMC9955174.
- [19] Xi Wang, Hao Chen, Caixia Gan, Huangjing Lin, Qi Dou, Efstratios Tsougenis, Qitao Huang, Muyan Cai, Pheng-Ann Heng, "Weakly Supervised Deep Learning for Whole Slide Lung Cancer Image Analysis," *IEEE Transactions on Cybernetics*, vol. 50, no. 9, pp. 3950-3962, Sept. 2020.
- [20] Jinzhu Yang, Bo Wu, Lanting Li, Peng Cao, OsmarZaiane, "MSDS-UNet: A multi-scale deeply supervised 3D U-Net for automatic segmentation of lung tumor in CT," *Computerized Medical Imaging and Graphics*, vol. 92, 2021.
- [21] Prasad Dutande, UjjwalBaid, Sanjay Talbar, "LNCDS: A 2D-3D cascaded CNN approach for lung nodule classification, detection and segmentation," *Biomedical Signal Processing and Control*, Vol. 67, May 2021.
- [22] Junli Tao, Changyu Liang, Ke Yin, Jiayang Fang, Bohui Chen, Zhenyu Wang, Xiaosong Lan, Jiuquan Zhang, "3D convolutional neural network model from contrast-enhanced CT to predict spread through air spaces in non-small cell lung cancer," *Diagnostic and Interventional Imaging*, Vol. 103, Issue. 11, pp. 535-544, November 2022
- [23] O. Ozdemir, R. L. Russell and A. A. Berlin, "A 3D Probabilistic Deep Learning System for Detection and Diagnosis of Lung Cancer Using Low-Dose CT Scans," *IEEE Transactions on Medical Imaging*, vol. 39, no. 5, pp. 1419-1429, May 2020.
- [24] Haichao Cao, Hong Liu, Enmin Song, Guangzhi Ma, Xiangyang Xu, RenchaoJin, Tengying Liu, Chih-Cheng Hung, "Multi-Branch Ensemble Learning Architecture Based on 3D CNN for False Positive Reduction in Lung Nodule Detection," *IEEE Access*, vol. 7, pp. 67380-67391, 2019.
- [25] Shweta Tyagi and Sanjay N.Talbar, "LCSCNet: A multi-level approach for lung cancer stage classification using 3D dense convolutional neural networks with concurrent squeeze-and-excitation module," *Biomedical Signal Processing and Control*, Vol. 80, Part. 2, February 2023.
- [26] S. Hemamalini , V. D. Ambeth Kumar , R. Venkatesan, S. Malathi. "Relevance Mapping based CNN model with OSR-FCA Technique for Multi-label DR Classification." *Journal of Fusion: Practice and Applications*, 11 no. 2 (2023): 90-110 (Doi : <https://doi.org/10.54216/FPA.110207>)
- [27] Hemamalini, Selvamani, and Visvam Devadoss Ambeth Kumar. 2022. "Outlier Based Skimpy Regularization Fuzzy Clustering Algorithm for Diabetic Retinopathy Image Segmentation" *Symmetry* 14, no. 12: 2512. <https://doi.org/10.3390/sym14122512>.
- [28] Kumar, V.D.A., Sharmila, S., Kumar, A. *et al.* A novel solution for finding postpartum haemorrhage using fuzzy neural techniques. *Neural Comput & Applic* **35**, 23683–23696 (2023). <https://doi.org/10.1007/s00521-020-05683-z>